Spring 2021

Spatiotemporal observations of water stress in Kansas winter wheat and corn from remotely sensed evapotranspiration and NDWI

Lindi Diane Oyler

Department:

SPATIOTEMPORAL OBSERVATIONS OF WATER STRESS IN KANSAS WINTER WHEAT AND CORN FROM REMOTELY SENSED EVAPOTRANSPIRATION AND NDWI

by

LINDI DIANE OYLER

A THESIS

Presented to the Graduate Faculty of the

MISSOURI UNIVERSITY OF SCIENCE AND TECHNOLOGY

In Partial Fulfillment of the Requirements for the Degree

MASTER OF SCIENCE IN GEOLOGY & GEOPHYSICS

2021

Approved by:

Ryan Smith, PhD, Advisor
Katherine Grote, PhD
David Borrok, PhD

ABSTRACT

Optimizing water use is a growing concern, especially in agricultural communities where water use is high. An important challenge in agricultural water optimization is knowing when and where crop water stress is occurring, particularly on large scales where in-situ measurements are no longer practical to obtain. In an effort to combat this challenge, this study utilizes remotely sensed evapotranspiration (ET) and Normalized Difference Water Index (NDWI) to evaluate the responses of integrated satellite datasets to water-stressed conditions over fields of irrigated corn, irrigated winter wheat, and rainfed winter wheat from 2007 to 2017 in southwestern Kansas. Using two different ET algorithms at various spatial resolutions, MOD16 and SSEBop, this research found that ET responses in water-stressed fields are lower in all three crop types with measurements of NDWI indicating lower crop water contents. Spatial resolution was found to be a critical factor in accurately separating the temporal signals of corn and winter wheat, as most MOD16 and SSEBop pixels contained a combination of various crops. After implementing additional filters that reduced the sample size only to fields with ≥90% pixel coverage over a single field of interest, the temporal trends better reflected trends found in previous studies and in Kansas crop growth manuals. Temporal trends of all three datasets suggest water stress can be quantified as an ET and NDWI deficit based on what is expected for each product. This study is a beginning step in determining quantitative criteria for "water stress" and how it appears in irrigated and rainfed crops through ET and NDWI datasets.

ACKNOWLEDGMENTS

First, I would like to thank my advisor, Ryan Smith, for his guidance, encouragement, and enthusiasm throughout the research process. Thanks for your support during my wacky highs, unfortunate lows, and numerous rabbit-hole adventures. We did it!

I would also like to express enormous gratitude to my parents for their personal support throughout my academic career. You fostered the curiosity and the critical thinking that made this thesis possible while managing to support me through two degrees with minimal debt. This will start us off in the real world so much farther than we ever could have hoped for. When we get that mountain-side hobbit hole in Colorado, you're welcome to visit anytime.

Next, I'd like to thank Jacob for his continued support through my entire graduate career. Love you bunches!

An additional thanks to Krista, Noor, Amanda, Shelby, Zach, and Josh. Party on, commune. Now we can have grilled chicken and movie nights without the fear of homework getting in the way!

Lastly, I would like to thank the hardworking crew of Giddy Goat Coffee House for brewing the perfect lattes and for greeting me with a smile when I became a regular during the writing process. Can I order London Fogs year-round now? I'll miss all of you.

TABLE OF CONTENTS

LIST OF ILLUSTRATIONS

Figure Page

LIST OF TABLES

NOMENCLATURE

Symbol	Description
ET	Evapotranspiration
ET_a	Actual evapotranspiration
ET_o	Short crop reference evapotranspiration
ET_r	Tall crop reference evapotranspiration
TWA	Total water applied
MODIS	Moderate Resolution Imaging Spectroradiometer
MOD16	MODIS Global Evapotranspiration Project
SSEBop	Operational Simplified Surface Energy Balance
METRIC	Mapping EvapoTranspiration at High Resolution with Internalized Calibration
NDVI	Normalized Difference Vegetation Index
NDWI	Normalized Difference Water Index
EVI	Enhanced Vegetation Inde
PRISM	Parameter-elevation Regressions on Independent Slopes Model
GEE	Google Earth Engine
USDA	United States Department of Agriculture
NASS	National Agricultural Statistics Service
CDL	Cropland Data Layer
USGS	United States Geological Survey

1. INTRODUCTION

Water resource management is becoming an increasingly important and complex area of study, especially in areas where optimizing water use is a growing concern. Water management plays a role in many broader issues such as food scarcity, groundwater scarcity, and climate change. These challenges are particularly important to address in agricultural areas—it is estimated that agriculture accounts for 90 percent of the world's total water consumption, two-thirds of the world's groundwater withdrawals, and one-third of total terrestrial evapotranspiration (Oki & Kanae, 2006). In the United States, irrigation accounted for 69% of total groundwater withdrawals in 2015. This equated to 57.2 billion gallons per day (compared to water pumped for domestic use—18.4 billion gallons per day). Despite the large volume of groundwater withdrawn from rapidly depleting aquifers in the United States, groundwater regulation is largely left to the states, leaving many groundwater withdrawals unmonitored altogether (Folger et al., 2020). However, advancements in remote sensing, data mining, machine learning, and cloud-based computing have made more frequent crop monitoring—and therefore, more frequent water management—a possibility on a global scale at a variety of spatial and temporal resolutions.

This study is part of a larger effort to integrate and evaluate remotely sensed datasets on the field, regional, national, and global scales in agricultural regions to investigate problems in monitoring crop water stress. Previously, studies have developed stress indices (such as the Crop Water Stress Index) or sought to use known indices (such as NDVI) to monitor crop health. The CWSI, primarily used for irrigation scheduling,

utilizes a relationship between canopy temperature, air temperature, and vapor pressure deficit to quantify crop water stress (Alderfasi & Nielson, 2001). The CWSI depends on two baseline values: a non-stressed threshold at which the crop is fully watered and a non-transpiring crop threshold in which the stomata are completely closed. Various implementations of this model have grown in complexity to include more environmental variables such as the crop minimum surface resistance at potential evapotranspiration or radiometric surface temperature (Yuan et al., 2004). The primary critique of the CWSI is its applicability across geographic locations, phenological stages, and even crop species and variety. Gardner and Shock (1989) proposed a range of vapor pressure deficits to accommodate changes in geographic location, but the stressed and non-water stressed baseline information is still not available in all locations (Alderfasi & Nielson, 2001). Alternatively, Normalized Difference Vegetation Index (NDVI) and Enhanced Vegetation Index (EVI) were developed to monitor plant chlorophyll content (vegetation growth) and canopy structural variations, respectively, using reflectances from near-infrared and red bands. When used in conjunction, they can monitor greenness while being able to distinguish between canopy and the background in high biomass regions (Huete et al., 2002). While plant growth and chlorophyll content can be used as a proxy for crop health, it cannot directly quantify crop water stress. NDVI is also prone to saturation in high biomass regions (such as agricultural regions) and has shown to produce a one month lag time between the onset of crop water stress and the appearance of the stress in the index (Huete et al., 2002; Ji & Peters, 2003).

This study mitigates issues posed by the CWSI and the use of NDVI and EVI by utilizing two remotely sensed global evapotranspiration (ET) algorithms and the

Normalized Difference Water Index (NDWI) to quantify crop water stress in winter wheat *(Triticum aestivum)* and corn *(Zea mays)* in Kansas from 2007 to 2017 (Figure 1.1). The two ET algorithms use many of the same inputs as the CWSI while accounting for other variables such as nighttime and daytime fluctuations in ET and lateral dispersion of heat across a landscape. NDWI uses two near-infrared wavelengths to monitor plant water content and has proven to be effective in high biomass regions like agricultural fields (Gao, 1996). Additionally, these datasets have a wide spatiotemporal range with global extents and temporal availability from 2001 to 2020. By integrating multiple remotely sensed datasets, this study can extend existing in-situ measurements and assist farmers with water management in regions where groundwater is increasingly scarce.

With this goal there are two major challenges: determining the amount of influence irrigation has on mitigating water stress and evaluating water stress in fields where irrigation may be occurring but is not monitored. To shed light on these issues, this study utilized a unique groundwater pumping dataset from the Kansas Geological Survey that contains annual withdrawal totals in irrigation wells from 1990 to 2017 (Wilson, 2019). Since most water uses in agricultural areas in Kansas are from groundwater, this dataset is a reasonable approximation for consumptive water use. It has provided insight into a major component of the hydrologic cycle that impacts water resource management—groundwater withdrawals specifically used for irrigation. This dataset addresses the first issue because it allows for distinction between rainfed and irrigated fields and the influence of water stress in each as it appears in ET and NDWI responses. Temporal trends of all three datasets over the decade suggest water stress can be

quantified as an ET and NDWI deficit based on what is expected for each product. The magnitude of the ET and NDWI deficit can also be an indicator of irrigation in winter wheat since deficits in rainfed winter wheat were greater than in irrigated winter wheat.

This study is a beginning step towards quantifying water stress and how it appears in irrigated and rainfed crops through ET and NDWI measurements. Having established a difference between irrigated and rainfed responses, this methodology could be applied in climatically similar regions where groundwater withdrawals are unmonitored.

Figure 1.1 Kansas (light blue) and the study area of southwestern Kansas (red). Map credits: ESRI, National Geographic, Garmin, HERE, UNEP-WCMC, USGS, NASA, ESA, METI, NRCAN, GEBCO, NOAA, Increment P Corp.

2. BACKGROUND

This background discussion begins with a fundamental concept that plays key roles in hydrologic cycle, water balance, and energy balance models: evapotranspiration. ET is defined as the sum of the return of vapor to the atmosphere from plant transpiration (evaporation within plant cells through the stomata) and evaporation or sublimation off land or water surfaces (Jensen & Allen, 2016). ET plays a major role in the hydrologic cycle. In the United States, it is responsible for 67 percent of the dispersion of precipitation whereas 29 percent is accounted for in surface water outflow, 2 percent is groundwater discharge, and 2 percent is used for human consumption. Of this proportion, transpiration accounts for more moisture returned to the atmosphere than evaporation from the soil and plant canopies. As factors such as cloud cover, vegetation density, surface reflectance properties, and the availability of solar energy change throughout the year, so does ET. Times of drought decrease overall ET because available soil moisture decreases and plants experience stomatal closure when water stressed (Hanson, 1991; Osakabe et al., 2014). Therefore, it is a vital component of the hydrologic cycle to account for when estimating past, present, and future water requirements for agricultural areas and municipalities. Estimating the largest transporter of moisture in the water cycle can help determine how much water is available and how much is still needed. This can be done using the water budget equation, shown in Equation 1:

$$P + GW_i - Q - ET - GW_o = \Delta S \quad (1)$$

where:

P = precipitation

GW_i = inward groundwater flow

Q = streamflow

ET = evapotranspiration

GW_o = outward groundwater flow

ΔS = change in water storage

The water budget equation is useful when there are few unknowns (areas where groundwater storage has been measured and groundwater use has been monitored, for example). However, this is commonly not the case. In large areas, field methods for estimating ET (such as lysimeters and eddy flux towers) become impractical.

Remote sensing technology has changed the way ET is estimated with sensors that measure many of the environmental variables included in the ET computation on a global scale with a reduced need for ground-based validation. The latest ET approaches rely heavier on the energy balance than the water balance because of this. Both ET algorithms discussed here begin with the conservation of energy. At the earth's surface, energy is partitioned into sensible heat flux (H), latent heat flux (λE), and available energy (A') by the energy balance equation (Equation 2) (Mu et al., 2017). Sensible heat flux is the conductive heat flux between the Earth's surface and the atmosphere, latent heat flux is the energy lost to the evaporation of water from the surface or transpiration from plants, and available energy is the sum of the sensible and latent heat fluxes (Mu et at., 2017; Stull, 2011; Tang & Li, 2014). The components that make up available energy (and therefore the sensible and latent heat fluxes) are net radiation (R_n), soil heat flux

(G), and heat storage flux (ΔS). Net radiation is the total radiation available after the differences between incoming and outgoing shortwave solar radiation and emitted and reflected longwave radiation are accounted for, soil heat flux is the amount of thermal energy moving through the soil per unit time, and heat storage flux is the amount of heat that flows into the ground during the day and is stored until it is conducted into the atmosphere at nighttime (Abtew & Melesse, 2013; Sauer & Horton, 2005; Kato & Yamaguchi, 2007).

$$A' = H + \lambda E = R_{net} - \Delta S_h - G \tag{2}$$

2.1. ACTUAL, POTENTIAL, REFERENCE, AND CROP ET

There are several key terms that must be discussed before algorithms for computing ET can be described in detail: actual ET, potential ET, reference ET, and crop ET.

2.1.1. Actual ET. Actual ET is the instantaneous ET at any point in time on a vegetated surface. There are several field methods for estimating ET such as weighing lysimeters and eddy covariance flux towers (though impractical for studying ET over large areas, these methods have been used to validate and ground-truth new ET algorithms). Many remotely sensed ET models use the Penman-Monteith equation as a basis for computing reference ET (which will be defined in Section 2.1.3) and ET fractions (which will be defined in Section 2.2.2 and shown in Equation 8). The challenge with using the Penman-Monteith equation is that it outputs an instantaneous actual ET for

one point on the surface. Empirically, latent heat flux can be computed with the Penman-Monteith equation as shown below in Equation 3:

$$\lambda E = \frac{\Delta(R_n - G) + \rho c_p (e_a - e_d)\left(\frac{1}{r_a}\right)}{\Delta + \gamma\left(1 + \frac{r_c}{r_a}\right)} \quad (3)$$

where:

r_c = canopy resistance

r_a = aerodynamic resistance

Δ = slope of the vapor pressure curve

R_n = net radiation

γ = psychrometric constant

G = soil heat flux

ρ = atmospheric density

c_p = specific heat of moist air

$e_a - e_d$ = vapor pressure deficit (saturation vapor pressure – actual vapor pressure)

λE = latent heat flux

The aerodynamic resistance term r_a can be computed as follows in Equation 4:

$$r_a = \frac{\ln\left[\frac{z_m - d}{z_{om}}\right] \ln\left[\frac{z_h - d}{z_{oh}}\right]}{k^2 u_z} \quad (4)$$

where:

r_a = aerodynamic resistance (s * m^{-1})

z_m = height of wind measurements (m)

z_h = height of humidity measurements (m)

d = zero plane displacement heigh (m)

z_{om} = roughness length governing momentum transfer (m)

z_{oh} = roughness length governing transfer of heat and vapor (m)

k = von Karman's constant, -0.41

u_z = wind speed at height ($m*s^{-1}$)

The bulk resistance term r_s can be computed as follows in Equation 5:

$$r_s = \frac{r_l}{LAI_{active}} \tag{5}$$

where:

r_s = bulk surface resistance ($s * m^{-1}$)

r_l = bulk stomatal resistance of the well-illuminated leaf ($s * m^{-1}$)

LAI_{active} = active (sunlit) leaf area index (m^2 * (leaf area) * m^{-2} (soil surface))

(Allen, 1998).

The psychrometric constant, γ, is a function of the specific heat of moist air, atmospheric pressure, the molecular masses of moist air and dry air, and the latent heat of vaporization (Mu et al., 2013).

Latent heat flux can then be converted to instantaneous actual ET by dividing λE by the latent heat of vaporization for water and the density of water and multiplying by the desired time unit (the time unit will depend on the algorithm and the sensor from which the latent heat flux is collected) (Irmak et al., 2012).

2.1.2. Potential ET. Potential ET is the ET that occurs on a vegetated surface with an unlimited water supply. It is the maximum possible ET for that surface. In an energy balance context, potential ET is where all available energy is consumed by the process of evaporating water and there is no energy left for sensible heat flux to the air (Irmak et al, 2012). One method for estimating potential ET is the Penman equation for evaporation over an open water surface (the results are then corrected for soil moisture).

2.1.3. Reference ET. Reference ET is a hypothetical ET value with respect to a well-watered certain type of vegetation such as grass or alfalfa at a known height (Tang & Li, 2014). While the reference ET value represents the potential ET with respect to a certain crop, the term is not interchangeable with potential ET. There are several equations for computing reference ET, but two of the most important are from the FAO-56 Irrigation and Drainage Paper Penman-Monteith equation and the ASCE Penman-Monteith equation (Allen, 1998; Allen et al., 2005). The FAO-56 Penman-Monteith Method involves inserting specific constants directly into the Penman-Monteith equation to compute ET for extensive green grass at a height of 0.12m, a constant latent heat of vaporization of λ=2.45 MJ kg^{-1} , albedo of 0.23, and a bulk surface resistance at 70 s m^{-1} for monthly, daily, and hourly time steps (Allen, 1998). The ASCE Standardized Reference ET equation was first introduced in 2005 in an effort to better account for ET differences between short and tall crops and to reduce confusion surrounding multiple equations for reference ET. Based on the concept of the FAO-56 method, the ASCE Standardized Reference ET equation combines the original Penman-Monteith, aerodynamic resistance, and bulk surface resistance equations and assumes crop height, latent heat of vaporization, and albedo to be constant. It also assumes that measurement

heights for air temperature and vapor saturation are 1.5 to 2.5m above ground, the wind speed is measured or adjusted to 2m height, and the weather measurements were collected over a grassy area with a vegetation height between 0.1 and 0.2 m. The equation is accompanied by a table, allowing one to adjust the constants to reflect both desired time step (hourly or daily) and approximate crop height. Short crops similar to grass measuring 0.12m will use the "short" reference ($\boldsymbol{ET_o}$) constants and tall crops similar to alfalfa measuring at 0.50 m will use the "tall" reference ($\boldsymbol{ET_r}$) constants. Constants for hourly time steps will also need to be adjusted for daytime or nighttime measurements (Allen et al., 2005).

2.1.4 Crop ET. Crop ET is defined as the ET from a "disease-free, well-fertilized crops, grown in large fields, under optimum soil water conditions, and achieving full production under the given climatic conditions" (Allen, 1998). It is computed by multiplying reference ET by the tabulated crop coefficient, $\boldsymbol{K_c}$, for a specific time in the growing season under dry or sufficiently moist conditions (Allen, 1998). Dry conditions require multiplying by a water stress constant, $\boldsymbol{K_s}$. It is important to know which reference ET equation one's desired ET model uses because different versions may require the use of a crop coefficient to compute crop ET while others may not.

2.2. ET ALGORITHMS

The two ET algorithms discussed here, MOD16 (MODerate Resolution Imaging Spectroradiometer (MODIS) Global Evapotranspiration Project) and SSEBop (Operational Simplified Surface Energy Balance), are the ones that were utilized in the investigative portion of this study. There are several other algorithms available for use

such as DisALEXI (Disaggregated Atmospheric-Land Exchange Inverse) and METRIC (Mapping EvapoTranspiration at high Resolution with Internalized Calibration), but because their temporal availability did not overlap with the temporal scope of the study, so they will not be discussed.

2.2.1. MOD16. The MOD16 ET model is the only Penman-Monteith-derived model that will be discussed in depth in this paper, but others include Priestly-Taylor and Blaney-Criddle. The common link between these models is their reliance on meteorological inputs to compute a reference ET. The appeal of MOD16 is its lack of assumptions about relationships between ET, moisture, and land surface temperature. Such independent measurements keep the model from relying too heavily on one input, but they can also be difficult to estimate (particularly surface resistance and aerodynamic resistance (the r_s and r_a terms defined in Section 2.1.1).

The fundamental concept of MOD16 is combining the drivers of evapotranspiration in a theoretically sound way that reduces bias and constrains the maximum ET rate with available energy. These drivers include land cover type, leaf area index, the fraction of absorbed photosynthetically active radiation (the ratio of incoming radiation to the radiation absorbed by plants), albedo (the fraction of solar radiation reflected by a surface), minimum temperature, vapor pressure deficit (the difference between saturation vapor pressure and actual vapor pressure), wind speed, and more mostly obtained from MODIS sensors (Mu et al., 2013; Wossenu & Melesse, 2013). In theory, over a moist surface where surface resistance is zero or significantly less than aerodynamic resistance, the equilibrium ET rate can be modeled as a function of the slope of the relationship curve between saturated water vapor pressure and temperature,

available energy, and the psychrometric constant. It is only limited by available energy. The equation for the equilibrium ET rate is the theoretical representation of potential ET (Equation 6).

$$\lambda E_{eq} = \frac{sA'}{\gamma} \tag{6}$$

where:

λE_{eq} = equilibrium ET rate

s = the slope of the relationship curve between saturated water vapor pressure and temperature

A' = available energy

γ = the psychrometric constant

When surface resistance is much greater than aerodynamic resistance, ET is controlled by surface resistance. It takes much more effort to return the moisture to the atmosphere. In this instance, ET is a function of the density of water, the specific heat capacity of water, vapor pressure deficit, the psychrometric constant, and surface resistance (Equation 7):

$$\lambda E_{rs} = \frac{\rho * c_p * (e_a - e_d)}{\gamma * r_s} \tag{7}$$

where:

λE_{rs} = ET that is controlled by surface resistance

ρ = atmospheric density

c_p = specific heat capacity of air

$e_a - e_d$ = vapor pressure deficit

γ = psychrometric constant

r_s = surface resistance

The previous version of the MOD16 algorithm (2007) held several assumptions that were changed in the Mu et al., 2011 update. The old algorithm assumed nighttime ET to be negligible and soil heat flux to be negligible on daily time steps in grassland and forest biomes. The 2011 update included a new nighttime ET component and a computation for soil heat flux as well as improved estimations of stomatal conductance, aerodynamic resistance, and boundary layer resistance, and separating the ET contributions between wet and dry canopy and wet and moist soil. The last improvement was made because there are differences in how evaporation and transpiration occur on wet and dry versions of the same surface (i.e. evaporation off a wet canopy as opposed to transpiration off a dry canopy). The difference between wet soil and moist soil is the accelerated rate of ET towards potential ET when soil saturation has been reached (wet) and the actual evaporation from the soil when there is a limited (but not negligible) water supply (moist) (Mu et al., 2013).

2.2.2. SSEBop. ET derived from combined surface energy balance methods and remotely sensed thermal data is a residual of solving, balancing, and partitioning the energy balance equation between sensible and latent heat fluxes. With these models, the Penman-Monteith equation is merely the first step in computing actual ET on a pixel-by-pixel basis. The advantage to these models over mass transfer models (which depend on Dalton's Law of partial pressures to estimate the net transfer of water vapor) and surface energy balance models that depend heavily on meteorological data (like MOD16) is their heavier reliance on remotely sensed data sources rather than ground measurements

(Abtew & Melesse, 2014). Additionally, models that combine the surface energy balance and thermal data contain fewer components and therefore, fewer sources of measurement error (Tang & Li, 2014).

The goal of the SSEBop approach to modeling actual evapotranspiration was to provide a 10-year average actual ET on regional and national scales for the conterminous United States. SSEBop ET_a is available at a 1km resolution over a variety of land cover types, performing best over urban areas, shrub land, and cropland. However, SSEBop is not able to distinguish the water sources of ET. For example, it cannot partition the amounts of ET that result from rainfall, irrigation, or soil moisture. Like many of its precursor models, SSEBop begins with computing the surface energy balance equation, reference ET, and an ET fraction (ET_f) on a pixel-by-pixel basis where the components are computed using meteorological data and thermal imagery. It is computed as follows in Equation 8:

$$ET_f = \frac{(T_h - T_s)}{(T_h - T_c)} \tag{8}$$

where:

$T_s =$ the observed land surface temperature of the observed pixel of interest (8-day average of a MODIS pixel)

$T_h =$ is the land surface temperature value of the "hot" reference pixel for the same 8-day time frame and the same scene

$T_c =$ is the land surface temperature value of the "cold" reference pixel for the same 8 day time frame and the same scene

Unlike ET algorithms that are derived from similar theory such as METRIC, SSEBop uses the ASCE Standardized Reference ET for a short crop at a height of 0.12m (i.e. grass). METRIC uses the tall crop version of the equation (i.e. alfalfa). SSEBop does not contain the internal calibration component that METRIC does, but it eliminates the need for the user to choose the upper and lower ET limits in a scene because it assumes a "hot" pixel has little or no ET occurring and a "cold" pixel represents potential (maximum) ET. The hot and cold limits are determined by a location's air temperature and energy balance computation at a given time. To account for spatial variability between hot and cold pixels, the algorithm utilizes a relationship between ET and land surface temperature (LST) to proportionally scale the values with respect to reference ET. The LST used in this process is an 8-day average of 1km MODIS pixels. The 8-day average lowers the influence of cloud cover. However, if clouds are prominent throughout the entire 8-day period, ET fraction values from one period previous or ahead is used to estimate ET fraction values for the missing period. Lastly, the 8-day 1km ET_a grids were computed by multiplying the ET fraction by the cumulative reference ET (Equation 9):

$$ET_a = ET_f \times ET_o \tag{9}$$

where:

ET_a = actual ET

ET_f = ET fraction

ET_o = cumulative grass reference ET over the 8-day time frame and scene of interest

SSEBop products are now available at daily, monthly, and annual time steps (Savoca et al., 2013; Senay et al., 2013). The algorithm proves quite useful in estimating water use for agriculture in arid regions where groundwater withdrawals for irrigation is the

dominant source of water. In these regions it is assumed that ET is representative of consumptive use--all the water applied is used in ET processes and none is returned to the system. However, this is a greater challenge in humid regions where groundwater withdrawals are supplemental to surface water, precipitation, and soil moisture (Savoca et al., 2013).

2.3. NDWI

The Normalized Difference Water Index (NDWI) is commonly used to estimate plant water content and has been used to supplement the Normalized Difference Vegetation Index (NDVI) to evaluate overall vegetation health. NDWI uses two near-infrared wavelengths at 0.86 micrometers and 1.24 micrometers and has been shown to penetrate high leaf area index zones (approximately eight leaf layers). These wavelengths are sensitive to plant water content because the absorption of liquid water at 0.86 micrometers is inconsequential and the absorption at 1.24 micrometers increases proportionally with the thickness of liquid water, so changes in the reflectance values in the 1.24 micrometer channel due to changes in plant water content are measurable. Additionally, these wavelengths sense similar depths within the canopy (for context, the red and near-infrared channels used in the NDVI calculation sense different depths, so the reflectance values represent those of different canopy thicknesses). Compared to the 1.5-2.5 micrometer range, liquid water absorption is significantly less in the 0.9 – 1.3 micrometer range and tends to saturate less even with higher leaf area indices, allowing for measurement of a wide range of liquid water content. Compared to NDVI, NDWI show a faster and greater response to drought conditions (Gao, 1996; Gu et al., 2007).

Additionally, NDWI experiences only minor effects from atmospheric water vapor. A limitation of NDWI is the influence of soil reflectance effects, especially in partially vegetated areas (Gao, 1996). The equation for the calculation of NDWI is given below:

$$NDWI = \frac{\rho(0.86\mu m) - \rho(1.24\mu m)}{\rho(0.86\mu m) + \rho(1.24\mu m)} \quad (10)$$

where:

ρ = reflectance value at each specified wavelength

2.4. CROP WATER REQUIREMENTS

Discussed here are the crop water requirements for winter wheat and corn as documented within the literature.

2.4.1. Winter Wheat. Since the 1980s, irrigated wheat acreage has held steady between 700,000 and 800,000 acres throughout Kansas, most of which is concentrated in the southwest portion of the state (Shroyer et al., 1997) Winter wheat is the second most irrigated crop behind corn, and it makes up one quarter of all irrigated Kansas crops. It has been shown that irrigation increases yield by 50 percent compared to rainfed yield, so irrigation is essential to the success of the crop in a region with relatively little precipitation. Winter wheat requires between 16 and 24 inches of water per year as it can consume 80 percent of available soil water before the soil moisture deficit starts impacting yield (Shroyer et al., 1997, Rogers, 1997).

Winter wheat has several growing stages beginning with planting in September and October. After tillering in the winter months, winter wheat begins "greening up" and growing again after having begun growing in the fall and surviving overwintering. The

cold is necessary for jointing and flowering in the spring as it initiates the change from vegetative growth (leaves) to reproductive growth (kernels). The next stages of boot, heading, and flowering involve extended growth of the plant's reproductive parts and pollination. The grain is produced during maturation two to four weeks after flowering (this can last up to twelve weeks if the weather is cool) (Shroyer et al., 1997).

Drought and excessive heat can seriously damage winter wheat by inhibiting starch production in the grains during maturation, causing the grains to shrivel and ripen prematurely. Wheat is harvested in June and July to avoid the worst temperature extremes, but hot and dry springs and early summers can still cause moisture stress. Winter wheat is relatively tolerant to moisture stress throughout its life cycle, but water during boot to heading (mid-May to mid-June) is most critical, requiring up to 0.5in (12.7mm) of water per day. Water application is next most critical during flowering, grain development in maturation (mid-June to mid-July), accounting for 38% of the total water applied for the season (Shroyer et al., 1997, Rogers, 1997).

2.4.2. Corn. Corn accounts for approximately half of the 3 million irrigated acres in Kansas and requires 22 to 30 inches (~560mm to 760mm) of water for full-season varieties (Rogers, 2007). Planting date is a critical factor to consider with different corn varieties. For southwest Kansas, the planting date occurs between April and May. Delayed planting may not allow the corn to fully mature and early planting may result in maturation during extreme heat as corn roots struggle to keep up moisture needs in temperatures greater than 86 degrees Fahrenheit. In a good year with plenty of spring rainfall and warm (but not extreme) weather in the summer, corn can produce 10 to 15

bushels per inch of total water applied (Roozeboom et al., 2007; Rogers, 2007; Duncan, 2007).

Corn's water needs depend greatly on growth stage, temperature, and soil moisture. During the germination and seedling stage, rainfall is often sufficient for providing soil moisture in finer-grained soils like those found in western Kansas. Areas with sandier soils may require earlier irrigation as they can have difficulty retaining water. The rapid growth stage results in leaves and roots growing quickly. As temperatures rise in western Kansas in June and mid-July, irrigation becomes necessary in the middle to late half of this stage. Corn is most sensitive to water stress during its reproductive stage, tasseling, and silking until pollination occurs in July. Once the corn reaches maturity and kernels have formed, water is still necessary to complete kernel development, but the most critical stage of water use is over (Rogers, 2007).

3. METHODS

3.1. DATA DESCRIPTION AND DOWNLOADS

The data acquired for this study were obtained through publicly available cloud-based platforms such as Google Earth Engine (GEE) (MOD16 ET, NDWI, PRISM precipitation), the USDA NASS CropScape download site (crop cover type), the USGS Early Warning System Monthly Actual ET download site (SSEBop), and the Kansas Geological Survey (groundwater pumping) (Earthdata Search, 2019; Gao, 1996; Daly et al., 2008, USDA, 2013, Senay et al., 2013; Wilson, 2019).

The cropland data layer (CDL) is a 30-m resolution raster derived from the Landsat 8 OLI/TIRS sensor, the Disaster Monitoring Constellation (DMC) DEIMOS-1 and UK2, the ISRO ResourceSat-2 LISS-3, and the ESA SENTINEL-2 sensors during the growing season of each year (2013 and later) (USDA, 2013). Datasets collected before 2013 were collected using the Landsat 5 TM sensor, Landsat 7 ETM+ sensor, and the Indian Remote Sensing RESOURCESAT-1 (IRS-P6) Advanced Wide Field Sensor (AWiFS) (USDA, 2010). We chose to exclude double cropped fields (wheat and corn, for example) so observations would be more representative of individual crops and to mitigate potential influence from larger resolution remotely sensed datasets. The SSEBop data was acquired as monthly actual ET estimates at a 1km resolution. The monthly total precipitation summations were acquired from 4km PRISM climate data via GEE (Daly et al., 2008). All the other datasets obtained with GEE were reduced to a monthly time step by taking the median value for each month at a 1km resolution. For example, if there

were two satellite passes for a particular month, the value that was acquired was the median of the two values. Below, Table 3.1 contains the details of each dataset.

Table 3.1 Datasets and their resolutions used in this study

Dataset	Product name	Spatial resolution	Temporal resolution	Acquisition Method	Unit	Conversion/ Scale Factor
MOD16 ET	MOD16A2.006 Terra Net Evapotranspiration 8-Day Global 500m	500m	8-day summation	GEE	kg/m^2/8day	.1 scale factor
NDWI	MODIS Aqua Daily NDWI	500m	Daily	GEE	Unitless, ranges -1 to 1	n/a
Precipitation	PRISM Monthly Spatial Climate Dataset AN81m	2.5 arc minutes (~4km)	Monthly summation	GEE	mm	n/a
SSEBop ET	USGS Early Warning System Actual ET	1km	Monthly	Direct download	mm	0.001 scale factor
Crop Data Layer	USDA NASS CropScape Downloader	30m	Annual	Direct download	Unitless (classification)	n/a
Groundwater withdrawals	Kansas Geological Survey	Point values	Annual	Provided in table format	Acre feet	Converted from acre-ft to mm/area in each pixel

The groundwater pumping dataset provided by the Kansas Geological survey contained annual total groundwater withdrawals (1990 to 2017) for municipal, irrigation, and stock water use as well as irrigated acreage. These were converted to points based on

locations of water diversions where a groundwater right permit was active or where water use was reported from (Wilson, 2019).

3.2. DATA REPRESENTATION

Differing spatial resolutions is a persistent challenge with gridded remote sensing data. Our resolution differences between cropland data layers, ET, and the groundwater pumping dataset posed questions of spatial accuracy within each field. For example, how is a point groundwater pumping dataset best represented over relevant fields? Also, there was the question of how to approach representation of ET values when there is overlap between the field extent and multiple pixel values. To combat the issue of different resolutions between data sources (particularly between the 30m CDL, 500m MOD16 ET, 1km SSEBop ET, and point dataset of groundwater pumping), the following approach was developed to best represent each dataset in the area covered by a particular crop. Each gridded dataset was converted to polygons at its native resolution and an area weighted average was computed over relevant fields.

3.2.1. Irrigated Crops. The groundwater pumping dataset was provided to us with geographic coordinates, total water pumped in acre-ft, acreage, and total water pumped for irrigation in acre-ft. To determine the groundwater pumping value at each point, the assumption of maximum potential coverage from each well was determined to be the irrigated acreage provided in the dataset. Wells with no pumping for a particular year were removed from the pumping dataset. We converted the pumping to a linear unit (millimeters) by dividing the amount of water pumped for irrigation by the area irrigated for the corresponding well and spatially assigned these points to the nearest CDL-derived

crop polygons within 250 meters (Figure 3.1). If there were several wells within the 250m boundary, all points were assigned to the polygon and averaged as they were aggregated.

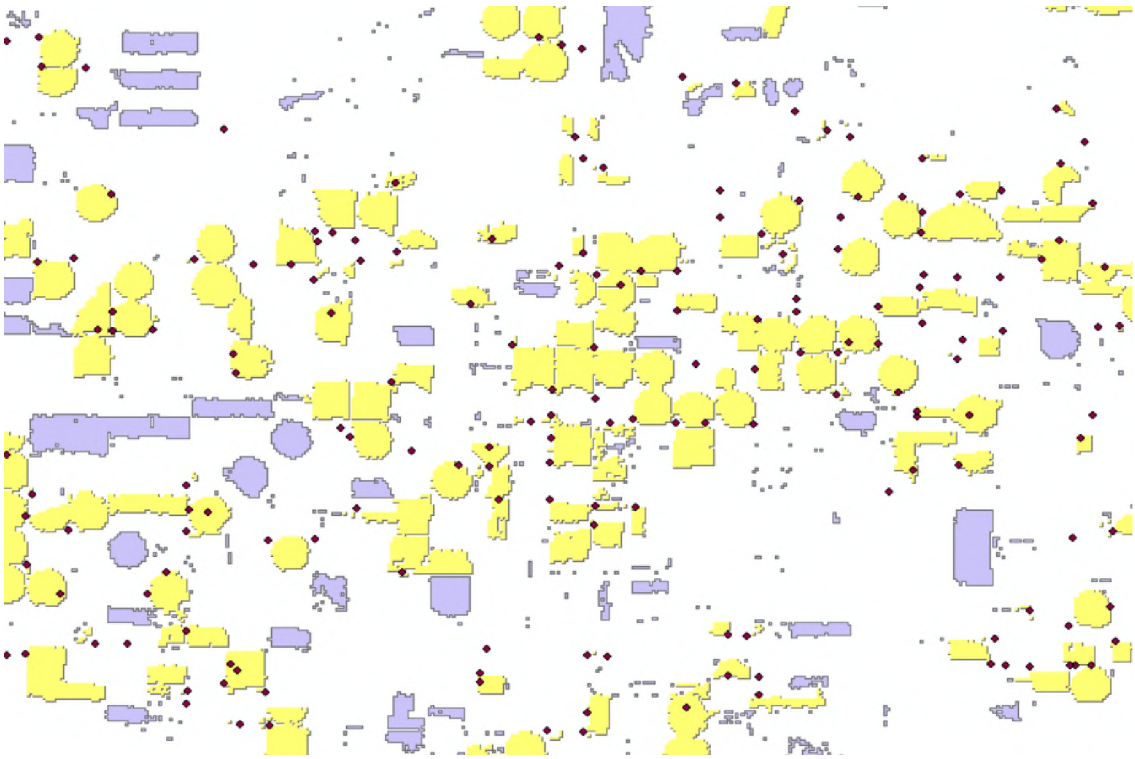

Figure 3.1 A visual representation of fields that are inferred to be irrigated, with wells within the 250m distance (yellow), and the fields that were presumed to not be irrigated or wells irrigating fields other than the ones of interest (purple)

From here individual parameter pixels were clipped to the field boundaries. Most pixels partially overlapped a single field, so an area weighted average was required to best represent the ET over each field. This was done by finding the area of each pixel fragment that covered a single field and dividing the fragment area by the area of the field. After multiplying the individual pixel values by this weight, the fragments were then merged to the shape of the field they covered and the sum of the weighted pixel

values was taken to represent the value of the entire field (this tool is called Dissolve in ArcGIS environments).

Lastly, data were classified into "sufficient" and "insufficient" watering. To establish these criteria, we developed a data-driven approach using the 10-year area weighted averages of total water applied (TWA) in irrigated fields. TWA is defined as the cumulative sum of precipitation and irrigation in irrigated fields and the cumulative sum of precipitation in rainfed fields. Any TWA pixels that fell in the bottom 10 percent of the 10-year TWA average was considered "insufficiently watered" and therefore "water-stressed" whereas anything above the 10^{th} percentile was considered "sufficiently watered" and "not water-stressed." This threshold was determined to be approximately the minimum recommended TWA amounts (550mm/year for irrigated corn and 515mm/year for irrigated winter wheat) (Rogers, 2007; Shroyer at al., 1997).

3.2.2. Rainfed Crops. For rainfed crops, we utilized the original CDL and applied the weighted average technique like that of irrigated crops. However, precipitation was the only water input for these fields and the fields determined "rainfed" were those that fell outside of a 250m radius of each well point. These data were also extracted into sufficient and insufficient TWA with TWA being derived from the area-weighted average of precipitation. Insufficient TWA corresponds to "water stressed" conditions that were found to be at or below the 10^{th} percentile total rainfall amount over the decade in the rainfed fields of interest. Sufficient TWA corresponds to "not water stressed" conditions and consists of PRISM area-weighted PRISM pixels that are above the same 10^{th} percentile cutoff. The 10^{th} percentile rainfed wheat cutoff was 400mm per

year, which is approximately 150mm lower than the recommended cumulative water application for winter wheat (Shroyer et al., 1997).

3.3. GEOSPATIAL ANALYSIS TOOLS

To conduct this study, we utilized geospatial analysis tools available in ArcMap and the R programming language. The statistical techniques, plots, and interpretations were conducted using the ggplot2 package in R.

4. RESULTS AND DISCUSSION

4.1. OBSERVATIONS OF TEMPORAL TRENDS

The observations from this section are derived from analyzing the changes in ET and NDWI under TWA conditions. The purpose of this analysis and the subsequent interpretations was to establish the difference between the algorithms in the context of water stress, namely determining how estimates from each ET algorithm were distributed throughout the growing season under various TWA conditions, how estimates from the ET algorithms compare across TWA conditions, what possible fundamental differences in the ET algorithms could cause differences that occur, and how the answers to these previous questions change when viewed in context with NDWI.

The first observation in addressing these questions was that the time series for each dataset were not always consistent with known growth patterns for the crops they represent (Figure 4.1). MOD16 and NDWI showed multiple peaks during each season for all crop types, which is inconsistent with the growth phenology of corn or wheat. SSEBop showed one peak, but the peak time does not change significantly between corn and winter wheat, although these crops are known to have different peak growth stages. Additionally, the NDWI signatures between irrigated wheat and rainfed wheat are inconsistent despite representing the same crop type. NDWI in rainfed wheat resembles that of irrigated corn more than irrigated wheat. The cause of this unusual trend in the timing and magnitude of ET and NDWI values could be the influence of irrigation. Overall, it makes sense that irrigation would produce higher ET and NDWI values, but

the increasing MOD16 and NDWI outside of the growing season is uncharacteristic of these crops.

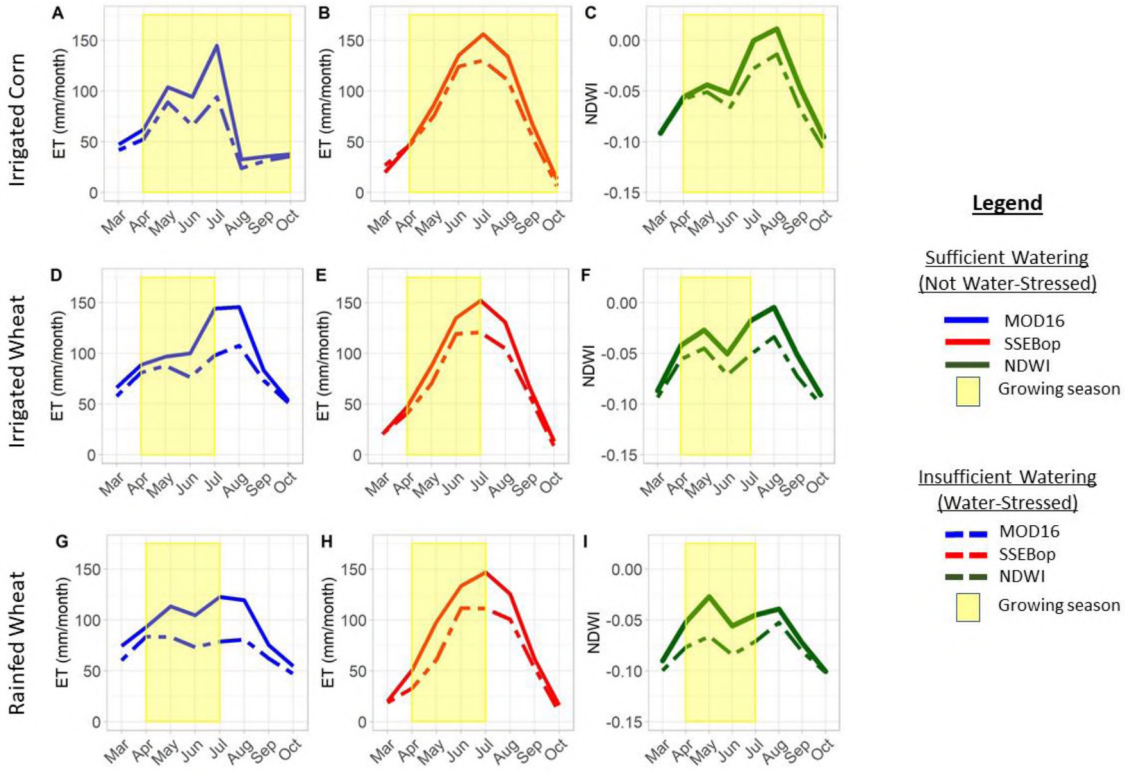

Figure 4.1 The resulting responses of MOD16, SSEBop, and NDWI in all three crop types under sufficient and insufficient watering conditions, corresponding to not water-stressed and water-stressed responses, respectively

Double-cropping can cause multiple growth peaks within a season. According to a study conducted by the United States Department of Agriculture, over the first half of this study's time frame (2007 to 2012), soybeans most commonly followed winter wheat in double-cropped fields. In the study region that included southwestern Kansas, 34 percent of double-cropped acres included soybeans (Borchers et al., 2014). This is one common practice of crop rotation and double cropping practiced with Kansas winter wheat. Others

include the wheat-fallow system (producing a wheat crop every two years) and wheat-summer crop-fallow system (produces two crops every three years) with summer crops including corn, sorghum, sunflower, and millet (Shroyer et al., 1997). One challenge in using MODIS data to visualize time series is that several fields fall within one pixel. To explore this issue using the magnitudes of NDWI data with different crops, 2017 Sentinel-2 NDWI, which has a 20 m, sub-field resolution, was derived over individual soybeans, sorghum, and double-cropped winter wheat/sorghum fields (Figure 4.2).

There were very few winter wheat/soy fields available, making it unlikely that

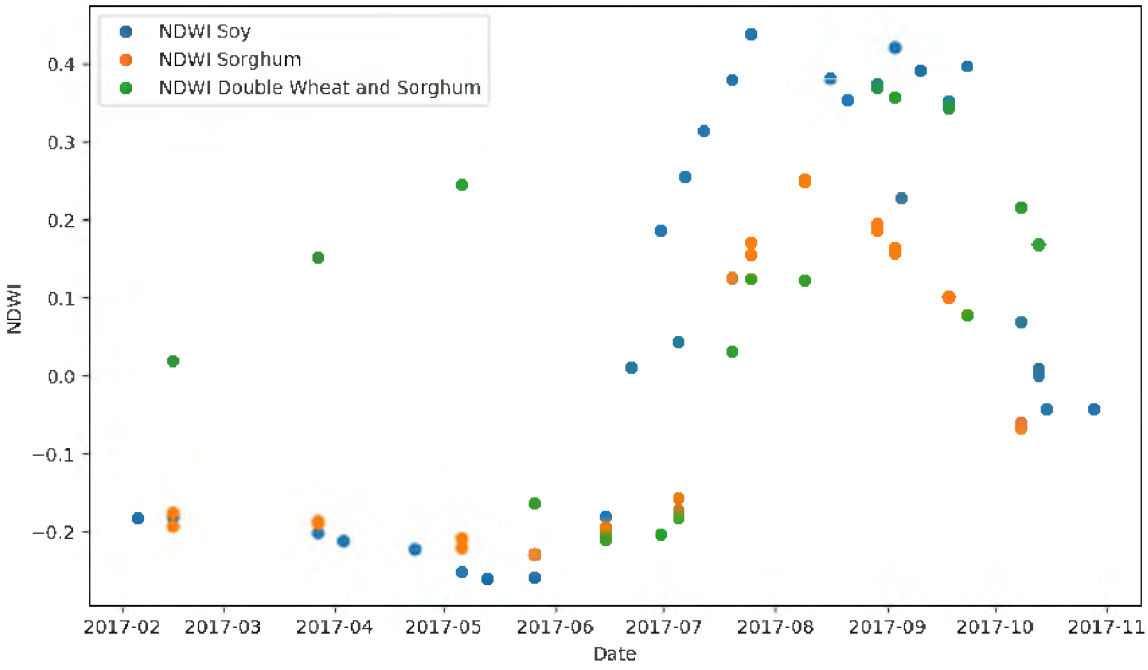

Figure 4.2 Sentinel-2 NDWI in 2017 over soybeans, sorghum, and double cropped winter wheat

this double cropping practice was the cause of such prominent double peaks. The time series shown in Figure 4.2 shows a double-peak in the double-cropped field that somewhat resembles that seen in Figure 4.1. However, without knowing the specific crop

rotations of each field, it is difficult to conclude crop rotations and undetected double cropping are the cause of the double peaks. In order for undetected double cropping to make such an influence on ET and NDWI responses, it would have to be a significant portion of fields. According to the 2017 CDL, approximately 1% of fields were classified as either double cropped winter wheat/soybeans or winter wheat/sorghum. This very small percentage, even with a compounded presence over the decade average if the wheat-summer crop-fallow crop rotation system was implemented, is an unlikely culprit of such influence on ET and NDWI responses.

It is more likely that spatial resolution differences between ET and NDWI products and field sizes cause the second out-of-season peak. With an average field size of 750m and not all pixels aligning directly with field boundaries, there is a high probability of influence from surrounding fields in the pixel on the final ET or NDWI value within each pixel. This can be seen well in Figure 4.3 where the Sentinel-2 NDWI

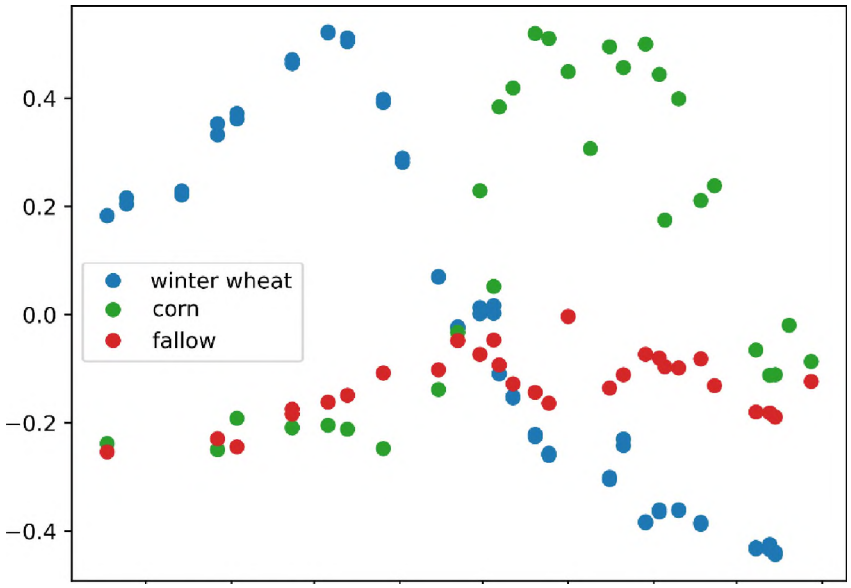

Figure 4.3 Sentinel-2 NDWI in 2017 showing winter wheat peaks in May and corn and fallow peaks in July – August in individual fields

peaks overlap in July. The peaks are distinct at a 20-m resolution, but this could easily be blurred at 500m and 1km spatial resolutions like those used by MOD16 and SSEBop.

This investigation into potential resolution issues was expanded to evaluate the spatial extent of influence from surrounding vegetation and its impact on the ET and NDWI readings for the entire study area. For each crop type, polygons of corn and winter wheat fields were derived from the 2014 CDL (2014 is a representative year for the decade of interest in terms of both temperature and precipitation). This investigation used fields classified in 2014 that overlapped with MOD16 and SSEBop pixels to maximize the interpretability of the results and to evaluate the effects at a 500m and 1km spatial resolutions. Fields were classified by watering technique (irrigated and rainfed) and then the fraction of the pixel covered by each crop of interest was computed by adding the total crop area from the polygons within the pixel and dividing it by the individual pixel area ($0.25km^2$ for MOD16 and $1km^2$ for SSEBop) (Figures 4.5 and 4.6).

These figures demonstrate that pixels that are entirely covered by a single crop type or even mostly covered by a single crop are quite uncommon. Because of its coarser spatial resolution, SSEBop has even fewer pixels with a high coverage fraction. Interestingly, the highest concentrations of high pixel coverage fractions in winter wheat appear in the northwesternmost and southeasternmost corners of the study area (also appearing consistently between MOD16 and SSEBop). This means that most pixels used in this study have multiple land use types contributing to their signal and explains why there are double-peaks in our time series—many pixels have both corn and wheat fields in them (Figure 4.4).

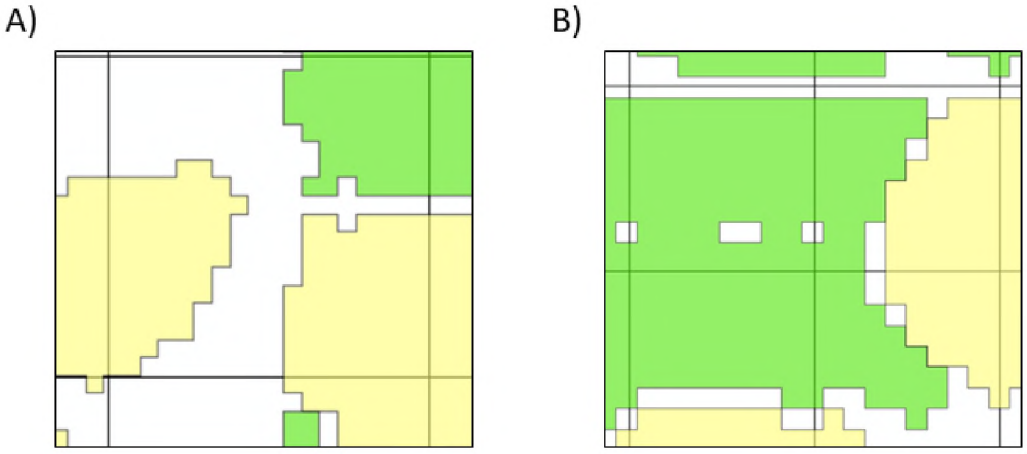

Figure 4.4 Field-scale influence from surrounding crops is present in both A) 1km SSEBop pixels and B) 500m MOD16 pixels with corn (yellow) and wheat (green)

This resolution issue was particularly prominent with winter wheat, which had an average fraction of pixel coverage of ~0.348 and ~0.273 for irrigated wheat and rainfed wheat, respectively. Corn had the highest fraction of pixel coverage of ~0.387. In summary, the resolution issue is extensive enough that over half of the ET and NDWI responses in each scene analyzed here are likely influenced by surrounding vegetation. To combat this issue, both MOD16 and NDWI were evaluated again in 2014 fields with over 90% pixel coverage by one crop of interest and SSEBop was evaluated again with over 75% pixel coverage, resulting in Figure 4.7. Figure 4.7 shows temporal trends that are closer to those suggested by Deines et al. (2017). Most notable are the higher overall peaks in irrigated corn and lowered double peaks in MOD16 and NDWI. While the first MOD16 and NDWI peaks in winter wheat better follow the expected temporal trends for the growing season, the continued presence of double peaks in general suggest that spatial resolution may still be an issue even with 90% or more of each pixel covering winter wheat.

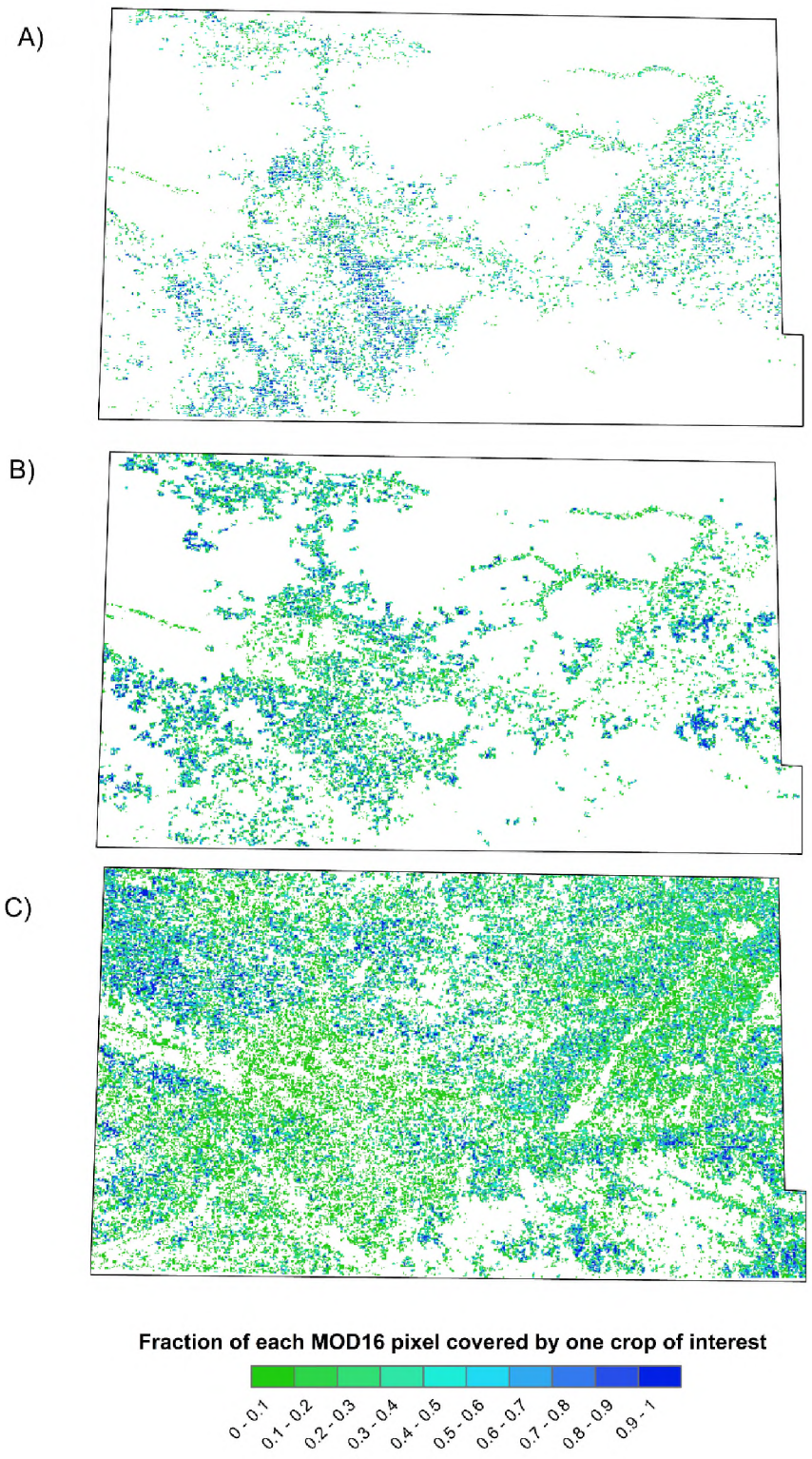

Figure 4.5 The spatial distribution of lead-over summarized as the fraction of each 2014 MOD16 pixel covered by A) Irrigated corn; B) Irrigated wheat; and C) Rainfed wheat

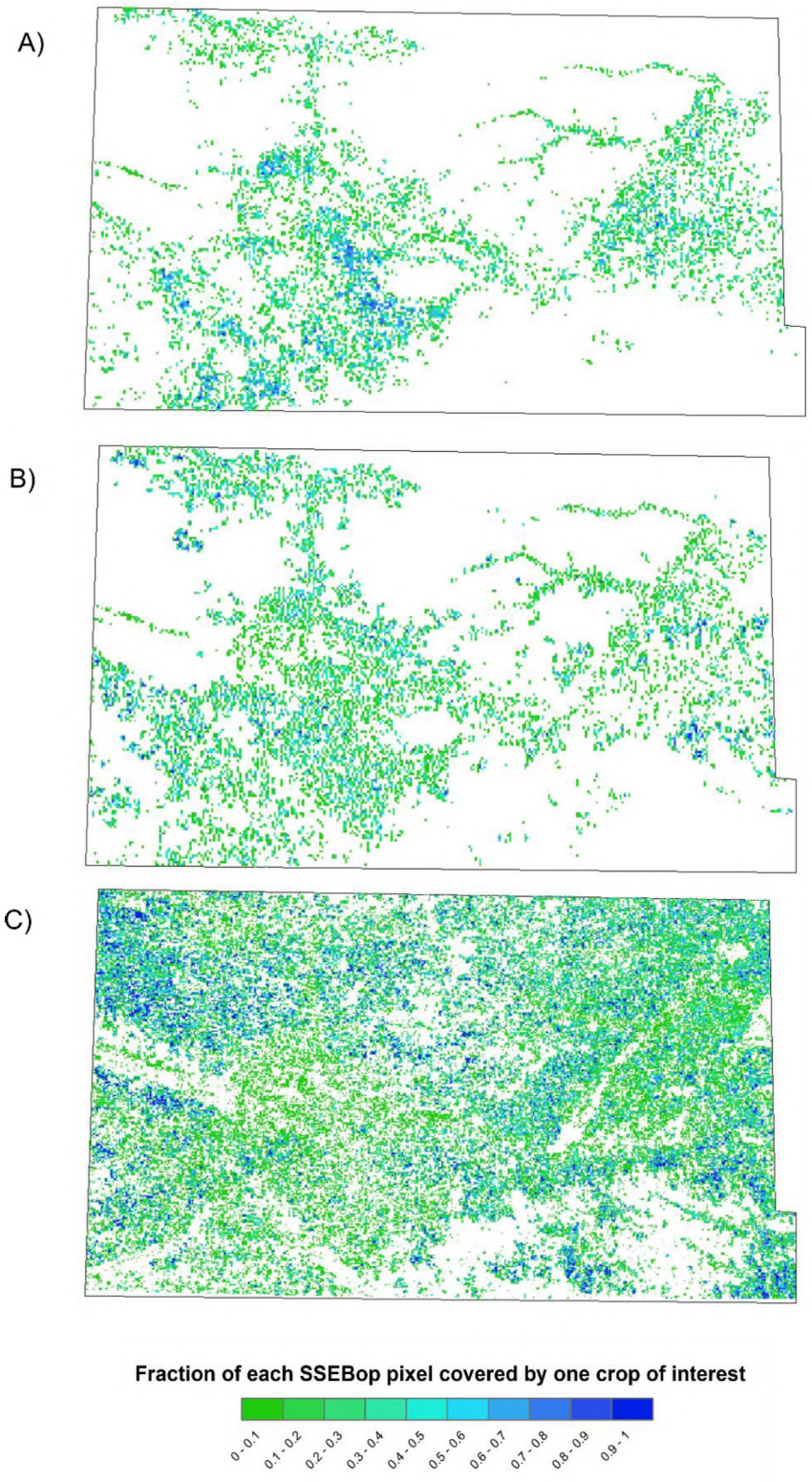

Figure 4.6 The spatial distribution of lead-over summarized as the fraction of each 2014 SSEBop pixel covered by A) Irrigated corn; B) Irrigated wheat; and C) Rainfed wheat

According to the MOD16 User's Guide, the input datasets used by the MOD16 algorithm have inconsistent spatial resolutions, ranging from half-degree (~50 km) GMAO/NASA meteorological data, 1 km albedo and the 0.5km MODIS pixel (Running et al., 2019; Strahler et al., 1999). The combination of inputs with varying resolutions could lead to a coarser 'true resolution' of MOD16 ET estimates. This may be the cause of double peaks still being present even after additional filtering. Persistent double peaks are less pronounced of an issue in corn, but that is likely because the water demand for corn in midsummer is high and corn produces strong ET and NDWI signals. SSEBop did not

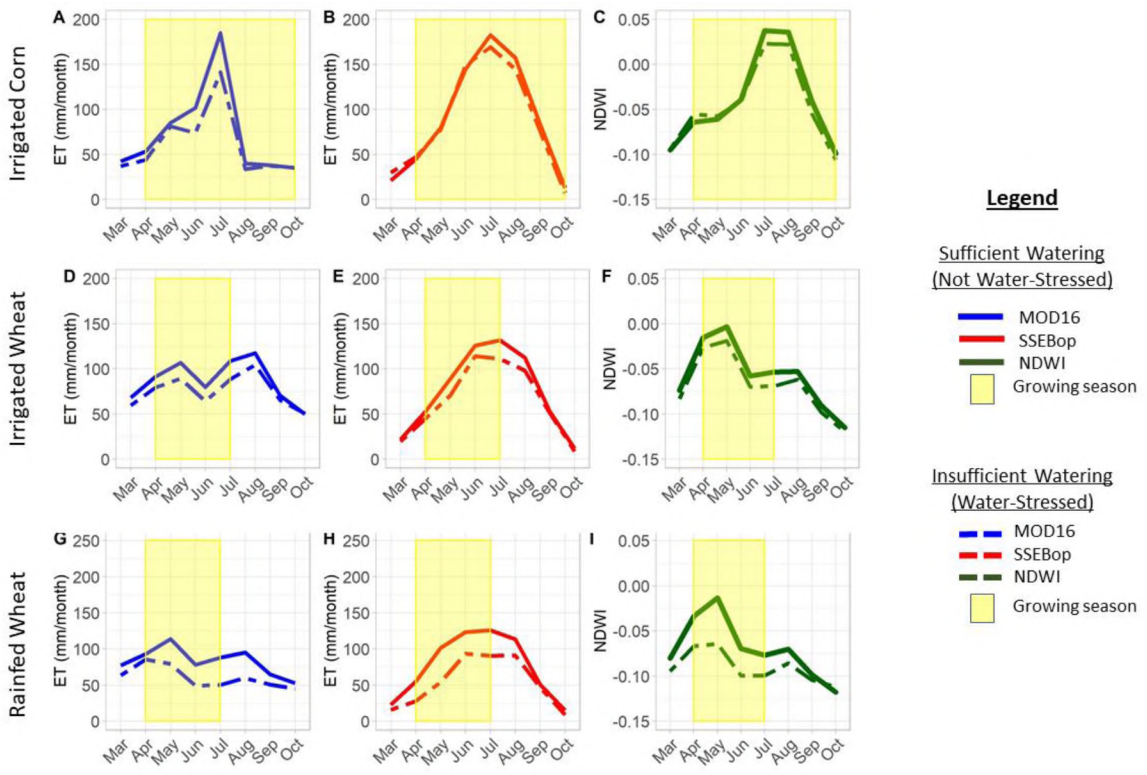

Figure 4.7 ET and NDWI evaluated again over fields with over 90% pixel coverage by one crop of interest in MOD16 and NDWI and 75% pixel coverage in SSEBop

improve as much as MOD16 and NDWI, likely because of the 1km spatial resolution. With an average field size of 750m, resolution issues were more prominent in SSEBop and the investigation resulted in significantly fewer available pixels from which to draw a trend. The original threshold of 90% lead to insufficient sample sizes when further filtering data into sufficiently watered and insufficiently watered categories over the decade. 75% pixel coverage was determined to be the next logical step. This threshold resulted in a larger sample size but potentially at the cost of clarity in the resolution investigation.

It can be seen that most insufficiently watered curves mirror the sufficiently watered curves, but at lower ET and NDWI values. This is not unexpected from a theoretical standpoint because water stress results in lower ET and plant water content. Furthermore, these results quantitatively determine the ET and NDWI deficits that occur due to water stress. Table 4.1 shows the average difference in ET and NDWI taken as the difference between the points of the average and low TWA points for each month and then averaged to a single value to represent the entire curve. As it can be seen from Table 4.1 and Figure 4.8, the rainfed wheat ET deficit is much larger in SSEBop and MOD16 ET (as compared to irrigated wheat and corn) and is comparable to the irrigated wheat deficit in NDWI. It appears that the rainfed wheat begins the growing season with an ET and NDWI deficit whereas irrigated wheat only develops deficits towards the growing season. This could be due to more water being applied to irrigated fields in the fall before winter dormancy. Application of water in the fall is important for ensuring well established crops and for maintaining soil moisture over the winter (Rogers, 1997). If there is already more of an abundance of moisture in irrigated wheat fields than rainfed

fields, then there is a larger supply of soil moisture for the crops to draw from at the most critical points in the season and that would appear as higher ET and NDWI with smaller deficits.

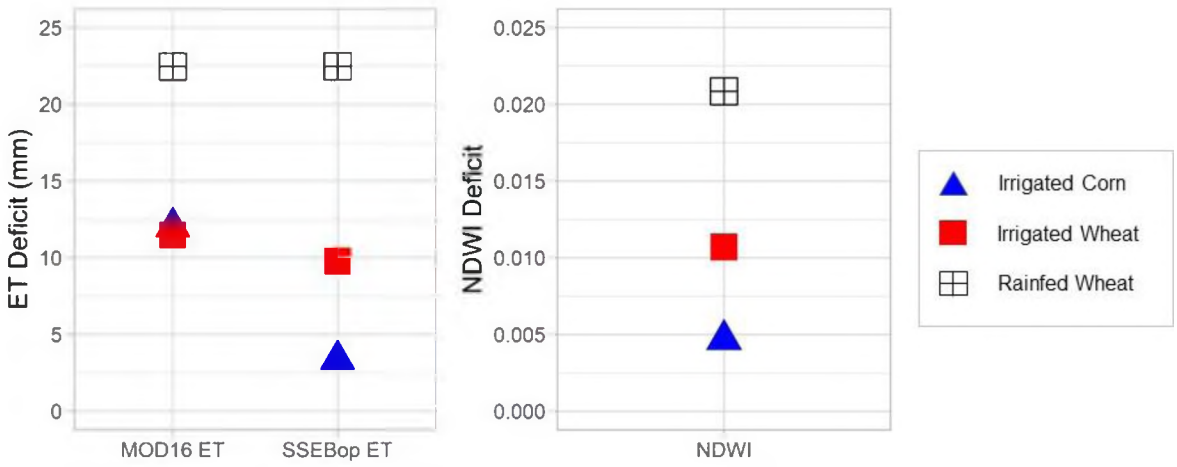

Figure 4.8 A visual representation of the results from Table 4.1

Table 4.1 Deficits in ET (mm) and NDWI due to water stress in fields with ≥90% pixel coverage with each crop

	MOD16 ET (mm)	*SSEBop ET (mm)*	*NDWI (unitless)*
Irrigated Corn	12.01	3.36	0.005
Irrigated Wheat	11.48	9.79	0.011
Rainfed Wheat	22.47	22.48	0.021

To summarize the results of this investigation, filtering pixels of MOD16 ET and NDWI with ≥90% coverage of one crop at a time yields trends that more accurately follow the expected trends of each crop over the growing season. Additionally, the effects of water stress are still apparent in all three parameters. In irrigated wheat and irrigated

corn, MOD16 and NDWI peaks are lower than anticipated. In rainfed wheat, the effects are even more dramatic with lower and earlier MOD16 peaks, possibly suggesting stunted growth or permanent damage to the crops caused by water stress. Although SSEBop results may be more heavily influenced by surrounding vegetation, Figure 4.7 still shows that water stress can result in lower than expected ET values.

4.2. UNEXPECTED DECLINES IN 2010

Additional plots show 2010 MOD16 with lower ET values than the severe drought years of 2011 and 2012. Figure 4.9 demonstrates this issue in MOD16 ET over corn fields (although the winter wheat fields show similar trends). The decline appears in

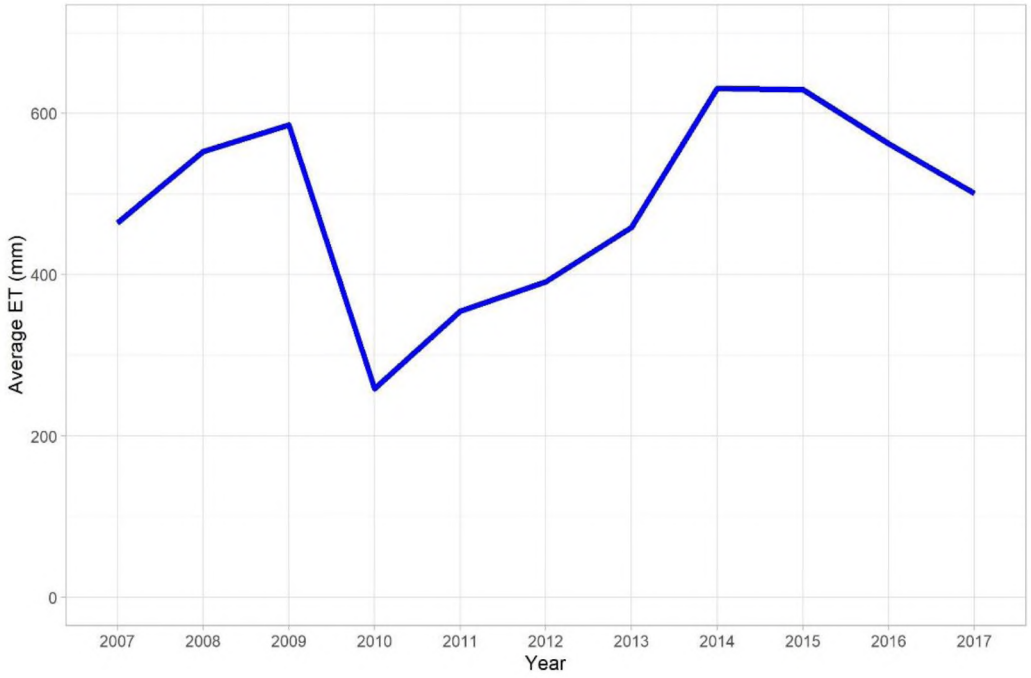

Figure 4.9 The decline in MOD16 ET over corn fields in 2010

both the unprocessed ET data (in which only a cloud mask is applied upon acquisition) and the processed data produced in this study (upscaled to a monthly time step), so the

issue could be attributed to cloud cover, an issue within the MOD16 algorithm in 2010, or factors undetectable by remote sensing such as disease and pests. Cloud cover influence was quickly ruled out as the QA statistics for the unmodified MOD16 ET products showed 2010 to be one of the best years for clear skies and good quality pixels in the study's time frame.

Investigating possible algorithm errors began with evaluating the performance of the land classification algorithm and potential influence of cloud cover. Running et al. (2017) suggested the importance of the MODIS land cover classification in the MOD16 ET computation cannot be overstated, but it is difficult to accurately classify land cover when many fields are smaller than the 500m MODIS resolution. This is a documented issue in the land classification User's Guide in which Sulla-Menashe and Friedl (2018) concluded that agricultural classifications are underrepresented. However, in viewing the differences in the MOD16 between grassland and cropland, it was found that the only difference is the closing vapor pressure deficits of 4200 and 4500 Pa, respectively--the vapor pressure deficit threshold at which plant transpiration stops due to stress from extreme temperatures or water availability (Running et al., 2017). The issue was investigated further by analyzing the proportion of "misclassified" fields in the region where "misclassified" is defined as a winter wheat field that is classified as something other than cropland (most commonly grassland). The results showed that winter wheat was more frequently classified as grassland than cropland, but this was not the case in 2010 more so than other years.

This leaves influence of factors beyond the scope of remote sensing. The evidence for disease influence is evident in NDWI, which does not depend on the MODIS land

cover classification. Despite good yields, a prominent disease in 2010 was stripe rust. The disease rate was significantly above the 20-year average and represented 76% percent of the year's disease loss with west central and northwest Kansas experiencing losses of 16% and southwest Kansas seeing a 6-8% loss. Strip rust is a fungus that thrives in cool and moist conditions like Kansas saw in early 2010 (Appel et al., 2010). At first it prevents the stomata from closing (which would result in an increase in transpiration) but then the leaves begin to die about 10 days afterwards (Rabbinge & Rijsdijk, 1981). This is the leading hypothesis for the decline in ET in 2010.

4.3. STUDY SOURCES OF ERROR

Potential sources of error for this study in general include contamination from surrounding fields in MODIS pixels, reporting bias in the groundwater dataset, our selected criteria for "water stress", and errors in the individual remotely sensed products. As it was found in the SSEBop ET dataset, influence from vegetation in surrounding fields can have an impact on the accuracy of the ET computation, especially later in the growing season when ET values from cropland are not as distinct from surrounding vegetation and crop fields. However, cataloguing these issues will help raise awareness of the issue for other long-term studies. Finer resolution products would be better spatial alternatives (especially when used with the 30m CDL), but they lack the temporal resolution necessary to view decade-long trends that extend before the 2010s, and they would require manual computation of ET. Trends in water stress can be analyzed at coarser resolutions if the potential issues are identified and accounted for.

Secondly, the groundwater pumping dataset is composed of self-reported values from farmers that were often rounded to the nearest whole number. This could result in an overall underestimation of groundwater pumping in the region, which could significantly compound when viewed on a regional scale. Additionally, although the criteria for "water stress" was data and literature driven, it is merely a starting point for determining what bounds of water stress might be. It was the goal of this study to view the extremes of water conditions, but plant stress is complex and might be influenced by other factors such as pests and disease.

Lastly, each remotely sensed product has its own potential sources of error. For example, the exact wavelengths of MODIS NDWI acquired from Google Earth Engine vary slightly based on which wavelengths are available at the time the image was produced. MOD16 and SSEBop have their own errors in the MODIS land classification algorithm, assumptions of linearity between NDVI and land surface temperature, and linear interpolation of ET values between pixels. The coarse resolution of PRISM and its interpolated production bring to question the field-scale accuracy of the product, but the spatial resolution works well enough for regional-scale analysis over the long term.

5. CONCLUSION

With evapotranspiration accounting for the return of more than 60 percent of precipitation over land and over 655,000 km^3/yr back to the atmosphere, its role in agriculture should be studied more in depth (Mu et al., 2013; Oki & Tanae, 2006). By gaining a thorough understanding of how ET behaves as the second largest component of the hydrologic cycle, we can use our observations to predict how it will behave in more extreme climatic conditions, saving time and money for all concerned (Oki & Tanae, 2006). With assistance from a unique dataset of groundwater withdrawals, this study established differences in MOD16 and SSEBop ET in irrigated corn, irrigated wheat, and rainfed wheat and found that there are quantifiable differences in ET and NDWI throughout all three crop types and watering conditions despite relatively coarse spatial resolutions, making them valuable tools for studying crop stress on a regional scale. MOD16 ET and NDWI were instrumental in distinguishing between rainfed and irrigated winter wheat with the rainfed wheat in water-stressed conditions.

To resolve issues of varying spatial resolutions and influence from surrounding vegetation, we implemented an additional data filter that reduced the sample size only to fields with ≥90% pixel coverage over a single field of interest. After implementing the filter, the temporal trends better reflected trends found in previous studies and in Kansas crop growth manuals. Both before and after the filter, however, the temporal trends suggested water stressed is a quantifiable variable, especially in winter wheat. The water stress is evident when we compare the ET difference between fields with greater than the 10^{th} percentile of water required by the crop and ET in fields with less than the 10^{th}

percentile of water required. NDWI can be used as a supplemental tool to evaluate the magnitude of water stress.

This study is a beginning step narrowing down quantitative criteria for "water stress" and how it appears through remotely sensed ET and NDWI datasets. Furthermore, quantifying the impact of spatial resolution issues and developing workarounds is another step forward in the remote sensing data mining effort that impacts the assessment of remotely sensed products in agricultural areas.

BIBLIOGRAPHY

Abtew, W., & Melesse, A. (2014). *Evaporation and Evapotranspiration: Measurements and Estimations*. Springer. doi:10.1007/978-94-007-4737-1

Alderfasi, A. A., & Nielsen, D. C. (2001). Use of crop water stress index for monitoring water status and scheduling irrigation in wheat. *Agricultural Water Management, 47*(1), 69-75. doi:10.1016/s0378-3774(00)00096-2

Allen, R. G. (1998). *Crop evapotranspiration: Guidelines for computing crop water requirements /cby Richard G. Allen* ... Rome: FAO.

Allen, R. G., Walter, I. A., Elliot, R. L., Howell, T. A., Itenfisu, D., Jensen, M. E., & Snyder, R. L. (2005). Appendix A - Description of Task Committee's Methodology and Procedures Used to Derive the Standardized Reference Evapotranspiration Equation. *The ASCE Standardized Reference Evapotranspiration Equation*. doi:10.1061/9780784408056.apa

Appel, J. A., DeWolf, E., Bockus, W. W., Todd, T., & Bowden, R. L. (2010). *Preliminary 2010 Kansas Wheat Disease Loss Estimates* (pp. 1-4, Rep.). Topeka, Kansas: Kansas Department of Agriculture.

Borchers, Allison, Elizabeth Truex-Powell, Steven Wallander, and Cynthia Nickerson. Multi-Cropping Practices: Recent Trends in Double Cropping, EIB-125. U.S. Department of Agriculture, Economic Research Service, May 2014.

Brooks, K. N., Folliott, P. F., & Magner, J. A. (2012). *Hydrology and the management of watersheds*. Retrieved from https://ebookcentral-proquest-com.libpro

Buja, A., Cook, D., Hofmann, H., Lawrence, M., Lee, E., Swayne, D. F., & Wickham, H. (2009). Statistical inference for exploratory data analysis and model diagnostics. *Philosophical Transactions of the Royal Society A: Mathematical, Physical and Engineering Sciences, 367*(1906), 4361-4383. doi:10.1098/rsta.2009.0120

Daly, C., Halbleib, M., Smith, J.I., Gibson, W.P., Doggett, M.K., Taylor, G.H., Curtis, J., and Pasteris, P.A. 2008. Physiographically-sensitive mapping of temperature and precipitation across the conterminous United States. International Journal of Climatology, 28: 2031-2064

Deines, J. M., Kendall, A. D., & Hyndman, D. W. (2017). Annual Irrigation Dynamics in the U.S. Northern High Plains Derived from Landsat Satellite Data. *Geophysical Research Letters, 44*(18), 9350-9360. doi:10.1002/2017gl074071

Duncan, S. R., Fjell, D. L., & Vanderlip, R. L. (2007). Growth and Development. In *Corn production handbook* (pp. 3-7). Manhattan, Kansas: Agricultural Experiment Station and Cooperative Extension Service, Kansas State University.

Earthdata Search. 2019. Greenbelt, MD: Earth Science Data and Information System (ESDIS) Project, Earth Science Projects Division (ESPD), Flight Projects Directorate, Goddard Space Flight Center (GSFC) National Aeronautics and Space Administration (NASA). URL: https://search.earthdata.nasa.gov.

Folger, P., Stern, C. V., Carter, N. T., & Stubbs, M. (2020). *The federal role in groundwater supply - R45259* (Version 5, pp. 1-34) (United States, Congressional Research Service). Congressional Research Service.

Gao, B. (1996). NDWI—A normalized difference water index for remote sensing of vegetation liquid water from space. Remote Sensing of Environment, 58(3), 257 266. doi:10.1016/s0034-4257(96)00067-3

Hanson, R. L. (1991). Evapotranspiration and Droughts. In R. W. Paulson (Author), *National water summary 1988-89: Hydrologic events and floods and droughts* (pp. 99-104). Washington, D.C.: United States Government printing Office

Huete, A., Didan, K., Miura, T., Rodriguez, E., Gao, X., & Ferreira, L. (2002). Overview of the radiometric and biophysical performance of the MODIS VEGETATION INDICES. *Remote Sensing of Environment, 83*(1-2), 195-213. doi:10.1016/s0034 4257(02)00096-2

Irmak, A., Kamble, B., Ratcliffe, I., Kjaersgaard, J., Huntington, J., Trezza, R., & Allen, R. G. (2012). *Operational Remote Sensing of ET and Challenges*. INTECH Open Access Publisher.

Jensen, M. E., & Allen, R. G. (2016). *Evaporation, evapotranspiration, and irrigation water requirements*. Reston, VA: American Society of Civil Engineers.

Ji, L., & Peters, A. J. (2003). Assessing vegetation response to drought in the northern Great Plains using vegetation and drought indices. *Remote Sensing of Environment, 87*(1), 85-98. doi:10.1016/s0034-4257(03)00174-3

Kato, S., & Yamaguchi, Y. (2007). Estimation of STORAGE heat flux in an urban area Using ASTER DATA. *Remote Sensing of Environment, 110*(1), 1-17. doi:10.1016/j.rse.2007.02.011

Mu, Q., Zhao, M., & Running, S. W. (2013). *MODIS Global Terrestrial Evapotranspiration (ET) Product (NASA MOD16A2/A3) Algorithm Theoretical Basis Document* (pp. 1-43, Rep. No. Collection 5). Missoula, MT: Numerical Terradynamic Simulation Group.

Oki, T., & Kanae, S. (2006). Global Hydrological Cycles and World Water Resources. *Science, 313*(5790), 1068-1072. doi:10.1126/science.1128845

Osakabe, Y., Osakabe, K., Shinozaki, K., & Tran, L.-S. P. (2014). Response of plants to water stress. *Frontiers in Plant Science*, *5*. doi: 10.3389/fpls.2014.00086

Rabbinge, R., & Rijsdijk, F. H. (1981). Disease and crop physiology: A modeller's point of view. In 1032707245 791556927 P. G. Ayres (Ed.), *Effects of Disease On the Physiology of the Growing Plant* (Vol. 11, S.E.B Seminar Series). Cambridge University Press. (*Disease and Crop Physiology: A Modeller's Point of View*, (1981), 201-220)

Rogers, D. H. (1997). Irrigation Management. In *Wheat Production Handbook* (pp. 29-31). Manhattan, Kan.: K-State Research & Extension.

Rogers, D. H. (2007). Irrigation. In *Corn Production Handbook* (pp. 30-36). Manhattan, Kansas: Agricultural Experiment Station and Cooperative Extension Service, Kansas State University.

Roozeboom, K., Devlin, D., Duncan, S., Olson, B., & Thompson, C. (2007). Optimum Planting Practices. In *Corn production handbook* (pp. 10-14). Manhattan, Kansas: Agricultural Experiment Station and Cooperative Extension Service, Kansas State University.

Running, S. W., Mu, Q., Zhao, M., & Moreno, A. (2019). *User's Guide MODIS Global Terrestrial Evapotranspiration (ET) Product (MOD16A2/A3 and Year-end Gap-filled MOD16A2GF/A3GF) NASA Earth Observing System MODIS Land Algorithm (For Collection 6)* (Vol. Version 2, pp. 1-38, User's Guide). National Aeronautics and Space Administration.

Sauer, T. J., & Horton, R. (2005). Soil Heat Flux. *Micrometeorology in Agricultural Systems, 47*, 131-154.

Savoca, M.E., Senay, G.B., Maupin, M.A., Kenny, J.F., and Perry, C.A., 2013, Actual evapotranspiration modeling using the operational Simplified Surface Energy Balance (SSEBop) approach: U.S. Geological Survey Scientific Investigations Report 2013-5126, 16 p., http://pubs.usgs.gov/sir/2013/5126.

Senay, G.B., S. Bohms, R. Singh, P.A. Gowda, N.M. Velpuri, H. Alemu and J.P. Verdin, 2013. Operational evapotranspiration mapping using remote sensing and weather datasets: A new parameterization for the SSEB approach. Journal of American Water Resources Research. In Press.

Shroyer, J. P., Whitney, D., & Peterson, D. (1997). Planting Practices. In *Wheat Production Handbook* (pp. 9-12). Manhattan, Kan.: K-State Research & Extension.

Stull, R. (2011). *Meteorology for scientists and engineers* (3rd ed.). Vancouver, BC: Dept. of Earth, Ocean & Atmospheric Sciences.

Sulla-Menashe, D., & Friedl, M. A. (2018, May 14). User Guide to Collection 6 MODIS Land Cover (MCD12Q1 and ... Retrieved October 27, 2020, from https://lpdaac.usgs.gov/documents/101/MCD12_User_Guide_V6.pdf

Tang, H., & Li, Z.-L. (2014). Quantitative Remote Sensing in Thermal Infrared. *Springer Remote Sensing/Photogrammetry*. doi: 10.1007/978-3-642-42027-6

USDA National Agricultural Statistics Service Cropland Data Layer. {2007 - 2017}. Published crop specific data layer [Online]. Available at https://nassgeodata.gmu.edu/CropScape/, (accessed Oct. 8, 2019; verified Feb. 13, 2021) USDA-NASS, Washington, DC.

Velpuri, N., Senay, G., Singh, R., Bohms, S., & Verdin, J. (2013). A comprehensive evaluation of two MODIS evapotranspiration products over the conterminous United States: Using point and gridded FLUXNET and water balance ET. *Remote Sensing of Environment, 139*, 35-49. doi:10.1016/j.rse.2013.07.013

Wilson, B. B. (2019). *Water Information Management and Analysis System (WIMAS) for the Web*. Lawrence, Kansas, USA: Kansas Geological Survey. http://hercules.kgs.ku.edu/geohydro/wimas/query_setup.cfm

Yuan, G., Luo, Y., Sun, X., & Tang, D. (2004). Evaluation of a crop water stress index for detecting water stress in winter wheat in the North China Plain. *Agricultural Water Management, 64*(1), 29-40. doi:10.1016/s0378-3774(03)00193-8

VITA

Lindi Diane Oyler earned their Bachelor of Science degree in Geology & Geophysics with emphases in Petroleum Geology & Geophysics and a Literature minor from Missouri University of Science and Technology in December 2019. They received a Master of Science degree in Geology & Geophysics also at Missouri University of Science and Technology in May 2021.